Heliyon 9 (2023) e15793

Contents lists available at ScienceDirect

Heliyon

journal homepage: www.cell.com/heliyon

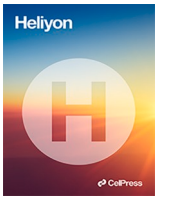

Research article

Ultrasensitive functionalized CeO_2/ZnO nanocomposite sensor for determination of a prohibited narcotic in sports pethidine hydrochloride

Suliman Y. Al Omar [a,*], Amal M. Al-Mohaimeed [b], Maha F. El-Tohamy [b,**]

[a] Doping Research Chair, Zoology Department, College of Science, King Saud University, Riyadh University, Riyadh-11451, Kingdom of Saudi Arabia
[b] Department of Chemistry, College of Science, King Saud University, P.O. Box 22452, Riyadh 11495, Saudi Arabia

ARTICLE INFO

Keywords:
Pethidine hydrochloride
Potentiometric sensors
Metal oxides
Nanocomposite
Polymeric sensors
Pharmaceuticals

ABSTRACT

The extraordinary features of cerium oxide (CeO_2) and zinc oxide (ZnO) nanostructures have encouraged substantial attention to those nanocomposites as probable electroactive complexes for sensing and biosensing purposes. In this study, an advanced novel factionalized CeO_2/ZnO nanocomposite-aluminum wire membrane sensor was designed to assess pethidine hydrochloride (PTD) in commercial injection samples. Pethidine-reineckate (PTD-RK) was formed by mixing pethidine hydrochloride and ammonium reineckate (ARK) in the presence of polymeric matrix (polyvinyl chloride) and *o*-nitrophenyl octyl ether as a fluidizing agent. The functionalized nanocomposite sensor displayed a fast dynamic response and wide linearity for the detection of PTD. It also revealed excellent selectivity and sensitivity, high accuracy, and precision for the determination and quantification of PTD when compared with the unmodified sensor PTD-RK. The guidelines of analytical methodology requirements were obeyed to improve the suitability and validity of the suggested potentiometric system according to several criteria. The developed potentiometric system was suitable for the determination of PTD in bulk powder and commercial products.

1. Introduction

Doping is currently a major topic at the international level in sports physiology. Not only are health issues at stake, but also the ethical ideals of humanity and honest team spirit in athletic competition. This has a direct impact on sports and competitions around the world [1,2]. In sport, doping refers to the use of illegal substances or practices to enhance performance [3]. The International Olympic Committee has declared this problem illegal and unethical. These committees regularly make serious allegations against such incidents that occur from time to time. This organization always makes great efforts to ensure that the sport is free from doping [4,5].

Pethidine hydrochloride (PTD) is a potent opiate analgesic used to treat many medical conditions [6]. Because PTD is also used illegally, it is on the controlled substance list (II) (drugs with high abuse potential but recognized medical purpose) in the United States

Abbreviations: ZnO, Zinc oxide; CeO_2, Cerium oxide; PTD, Pethidine hydrochloride; PVC, Polyvinyl chloride; O-NPOE, o-nitriphenyloctyl ether; ARK, Ammonium reineckate.

* Corresponding author.
** Corresponding author.
E-mail addresses: syalomar@ksu.edu.sa (S.Y. Al Omar), muhemeed@ksu.edu.sa (A.M. Al-Mohaimeed), moraby@ksu.edu.sa (M.F. El-Tohamy).

https://doi.org/10.1016/j.heliyon.2023.e15793
Received 1 February 2023; Received in revised form 13 April 2023; Accepted 21 April 2023
Available online 26 April 2023

and many other countries. Pethidine is commonly used in medicine as a postoperative analgesic and is also administered as an alternative to heroin [7]. In order to perform better in competitions, athletes often take pharmacological doses that are significantly higher than those prescribed for therapeutic purposes or in clinical research.

The International Olympic Committee and other sports have banned its use [8]. Therefore, the determination of pethidine has significant practical implications. Numerous sophisticated analytical approaches exist for the determination of pethidine, including high-performance liquid chromatographic analyzes [9–12], spectroscopic methods [13], and electrochemical and potentiometric methods [14–22]. Numerous of these techniques require various elaborate manipulations, extraction steps, and derivatization reactions that are susceptible to a variety of interferences and are not suitable for colored or turbid solutions.

Potentiometric sensors have the advantages of simple design, fabrication and handling, excellent selectivity, fast dynamic response time and applicability to colored and turbid solutions [23]. Also, due to their possible interfacing with automated and computerized systems, they have proven useful for the analysis of pharmaceutical formulations and biological samples [24,25]. Several sensors have been developed for the determination of pethidine hydrochloride, but they still have certain limitations. A recipe is clearly needed for the preparation and development of potentiometric sensors with low detection limits, high stability and reproducibility [14–22].

Nanocomposite is a reactive nanomaterial with numerous design and combination possibilities. Due to their growing demand and rapid research to fabricate sensors, their potential is so great that they can be effectively used in a variety of sensing and biosensing approaches [26]. Indeed, they have emerged as viable alternatives to compensate for the drawbacks of microcomposite materials. These materials also possess exceptional structural and optical qualities that are not present in conventional types [27]. Moreover, the fabrication of nanocomposites is considered a crucial step in the development of various electronic devices [28], targeted drug discovery systems [29], and biomedical probes [30].

Currently, many studies are being conducted on metal oxides, including copper oxide (CuO), zinc oxide (ZnO), and cerium oxide (CeO_2). Cerium oxide (CeO_2) is also increasingly used in various industries, such as catalysis, packaging, biomedical, and sensing [31–34]. Recently, there has been an increased interest in the preparation of zinc oxide nanoparticles (ZnONPs) with high specific surface area, thermal stability, and exceptional catalytic, conductive, and optical properties for advanced engineering and industrial applications [35]. A successful synthesis of CeO_2/ZnO nanocomposites with an environmentally friendly approach has been described, recommending the use of CeO_2/ZnO nanocomposites in electrochemical sensing applications [36].

The use of consumable plant waste for material synthesis and production is known to be highly sustainable with little or no negative impact on natural resources, the environment, organisms, and people. Although some claim that the impact of agricultural waste on human health and the environment is not comparable to that of conventional waste, sustainable ideologies aim for little or no waste generation [37–39]. Consequently, recycling or reusing agricultural waste can help save the ecosystem from depletion and degradation [40].

In this study, we demonstrate the environmentally safe conversion of barley and rice husk wastes into metal oxide nanomaterials. Several studies have reported the use of barley and rice husks for the green synthesis of nanoparticles used in various fields such as photocatalysis, biomedicine, and biosensing [41–47]. The phytochemicals of barley and rice husks, such as phenolic compounds, lignans, tocols, flavonoids, and folates [48], can act as reducing, capping, and stabilizing agents in the synthesis of nanoparticles [49].

The aim of this research is to use natural plant husk extracts from barley (*Hordeum vulga*re) and rice (*Oryza sativa*) for biogenic synthesis of CeO_2/ZnO nanocomposites. The nanocomposite was used to prepare a newly developed polymeric pethidine hydrochloride pure CeO_2/ZnO (PTD-RK -CeO_2/ZnO) nanocomposite sensor for potentiometric measurement of a banned anesthetic in sports pethidine hydrochloride in its real and pharmaceutical injections.

2. Experimental

2.1. Chemicals

Naturally prepared barley (*Hordeum vulgare*) and rice (Oryza sativa) husk extracts were used in this study to synthesize eco-friendly metal oxide nanoparticles (Cerium oxide and zinc oxide nanoparticles (CeO_2NPs and ZnONPs), respectively. The chemical substances including, sodium hydroxide (99.0%), zinc sulfate (99.9%), and cerium nitrate hexahydrate (99.9%) were provided by (WinLab, New Jersey, United States). Ammonium reineckate mono hydrate salt (ARK), polymeric material (polyvinyl chloride, PVC), *ortho*-nitrophenyl octyl ether (*o*-NPOE), as well as solvents such as tetrahydrofuran (THF, 97.0%), acetone, (99.9%) methanol (99.9%), and ethanol (99.9%) were purchased from (Sigma-Aldrich, Hamburg, Germany). Pethidine® injections (50 mg/1 mL, Roche, Basel, Switzerland) were purchased from local drug stores.

2.2. Instrumentation

The analytical investigations were established using new designed potentiometric functionalized CeO_2/ZnO nanocomposite sensor in conjunction with reference one (Ag/AgCl) and connected with the HANNA-211 instrument for potential difference readings (Smithfield, Rhode Island, United States). The analytical measurements were carried out using a potentiometric system comprises of a reference electrode (silver/silver chloride), a fabricated indicator sensor, and a digital HANNA 211-pH meter (Smithfield, RI, USA). The pH optimization throughout the analytical studies was performed using Metrohm-744 (Herisau, Switzerland) pH-meter. To confirm the pre-synthesized metal oxide nanoparticles, various instruments were used including Perkin-Elmer-spectrometer (Waltham, USA), Shimadzu-spectrophotometer (Kyoto, Japan), JSM-7610F scanning electron microscope (SEM, Tokyo, Japan), Shimadzu X-ray diffractometer-6000 (Kyoto, Japan). The elemental composition was determined using Energy-Dispersive X-Ray Spectroscopy

(EDX, Tokyo, Japan).

2.3. Preparation of barley (*Hordeum vulgare*) and rice (*Oryza sativa*) husk extracts

The husks of barley and rice were collected separately and sieved to remove any contaminated substances. Then the collected husks were washed 6 times with distilled water to remove any remaining impurities. A hot air oven was used to dry the washed husks at 70 °C for 24 h. The dried husks were refined to a size 50–200 μm and approximately 30 g of the dried powder husks were heated in 300 mL distilled water at 60 °C for 2 h under constant magnetic stirring. Then filtered using Whatman filter paper No. 40. The obtained extract of each husk was stored in an Erlenmeyer flask at 4 °C for further use in the synthesis of metal oxide nanomaterials [50].

2.4. Green synthesis of CeO_2 and ZnO nanoparticles

To synthesize CeO_2NPs and ZnONPs, 50 mL of barley and rice husk extracts were heated for 30 min at 60 °C. Then the hot extracts were mixed separately with 250 mL of (0.5 mol L^{-1}) solution of cerium nitrate hexahydrate or zinc sulfate. The mixture was heated for 2 h at 80 °C under proper agitation (750 rpm) for 30 min. The formed precipitates of CeO_2NPs and ZnONPs were separately recovered by centrifugation at 6000 rpm for 10 min, filtered using Whatman filter paper No. 1, and washed using deionized water three times to remove any residual extract. The produced nanomaterials were air oven-dried at 100 °C (Scheme 1) [51].

2.5. Preparation of analytical samples

Different analytical samples with desired concentrations (1.0×10^{-8}-1.0×10^{-2} mol L^{-1}) were prepared after serial dilution of a standard PTD solution (0.284 g in 100 mL distilled water) using distilled water.

2.6. Fabrication of PTD-RK sensors

The ion-pair complex (PTD-RK) was created by combining equivalent amounts and concentrations of each PTD drug solution and a precipitating agent RK (50 mL, 1.0×10^{-2} mol L^{-1}). The resulting electroactive complex PTD-RK was kept aside to dry overnight at room temperature after being rinsed three times with distilled water and collected by filtration using Whatman filter paper No.1.

PTD-RK (10 mg), PVC (190 mg), and *o*-NPOE (0.4 mL) were combined with 50 mL of the organic solvent THF to create the coated membrane PTD-RK and PTD-RK-CeO_2/ZnO nanocomposite. The membrane material was then poured into a round Petri plate with a diameter of 3 cm, and it was left to dry until an oily mixture had formed. To create the coated sensor PTD-RK, a pure Al wire was polished, washed three times with acetone, and then dipped in the membrane mixture several times to form a thick coated layer. The ultrasensitive PTD-RK-CeO_2/ZnO nanocomposite sensor was prepared by following the above-discussed procedures but 10 mg of CeO_2/ZnO nanocomposite was added and kept for15 min under constant stirring to well-dispersed and homogeneous membrane matrix. The functionalized mixture was used to coat the Al wire, and the sensors were then allowed to dry overnight at ambient temperature. The sensors were then preconditioned by soaking them separately in 1.0×10^{-3} mol L^{-1} PTD solution. Scheme 2 demonstrated the potentiometric system and the ultrasensitive functionalized PTD-RK-CeO_2/ZnO active sites PTD interaction.

2.7. Calibration graphs

A calibration plot is a common and significant step in analytical methodologies to evaluate the findings obtained. In the current study, the calibration graphs were plotted using 50 mL of 10×10^{-5}- 10×10^{-2} and 10×10^{-8}- 10×10^{-2} PTD solutions and the potential readings were recorded using PTD-RK and PTD-RK-CeO_2/ZnO nanocomposite sensors, respectively. The calibration graphs represent the potential readings of the developed sensors vs. the concentration of PTD solutions. The resulting plots were fitted and the regression equations were derived.

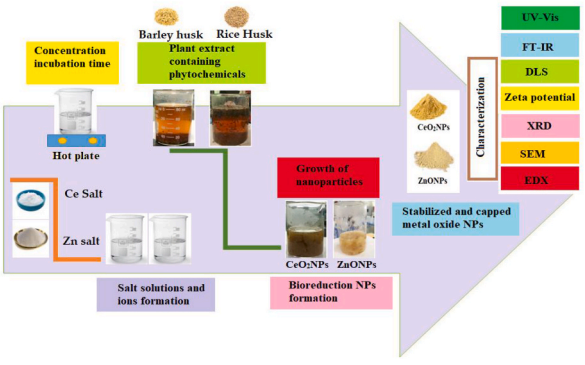

Scheme 1. Biogenic synthesis of CeO_2NPs and ZnONPs using barley and rice husk extracts, respectively.

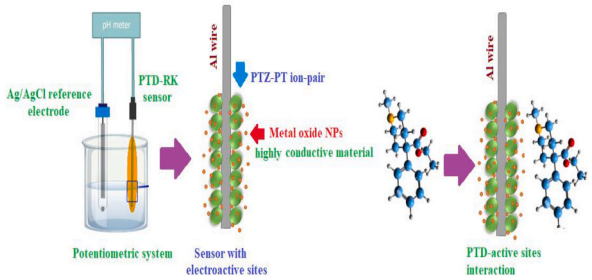

Scheme 2. The potentiometric system and the PTD active sites interaction.

2.8. Adjustment of analytical conditions

Several variables such as dynamic sensor response, selectivity, degree of sensitivity, and pH should be studied and addressed because they could alter sensor behavior.

The primary focus of coated wire sensors is the development of extraordinary transducer materials. Conceptually, these materials produce operationally consistent and have additional qualities for the coated sensors, including portability, exceptional flexibility, and maintenance-free operation. Better transducer materials including conducting polymers, carbon-based materials, and other common metal and metal oxide nanomaterials have been focused in numerous studies [52]. By observing the potential response of 1.0×10^{-8}-1.0×10^{-2} mol L^{-1} of PTD solutions, the response time was calculated.

The pH is one of the most important parameters that should be optimized to detect the suitable pH range of the designed sensors. For this purpose, 50 mL of PTD (1.0×10^{-4} mol L^{-1}) was analyzed using the suggested PTD sensors by changing the pH of the test solution from acidic to alkaline slightly adding a few drops of hydrochloric acid or sodium hydroxide (0.1 mol L^{-1}). Three sensors were connected to the PTD-RK or PTD-RK-CeO_2/ZnO nanocomposite, Ag/AgCl reference electrode, and combined glass electrode for pH measurements. Then to determine the independent pH values for the intended sensor, the pH values vs. the potential measurements (mV) were plotted [53].

In analytical detection, the most significant aspect that could influence the sensor's potential response is its selectivity. To assess the selectivity coefficient of the proposed sensors, a separate solution technique [54] was frequently used. The selectivity coefficient K^{pot+} was calculated by measuring the sensor's potential readings in 1.0×10^{-3} mol L^{-1} of each PTD solution and any probable foreign chemicals separately, such as certain cations, amino acids, polysaccharides, sugars, and coformulation additives. The previously published equation [55] was used to get the tolerable values.

2.9. Analytical determination of PTD in commercial injection

The content of 20 ampules was mixed well in a beaker and an equivalent amount to prepare 1.0×10^{-2} mol L^{-1} of PTD stock solution was transferred to a 100-mL volumetric flask and directly diluted to volume using distilled water. Serial dilution was carried out using distilled water to produce 6 different concentrations (1.0×10^{-7}-1.0×10^{-2} mol L^{-1}).

The suggested PTD-RK and PTD-RK-CeO_2/ZnO nanocomposite sensors were used to analyze each sample using direct potentiometric detection.

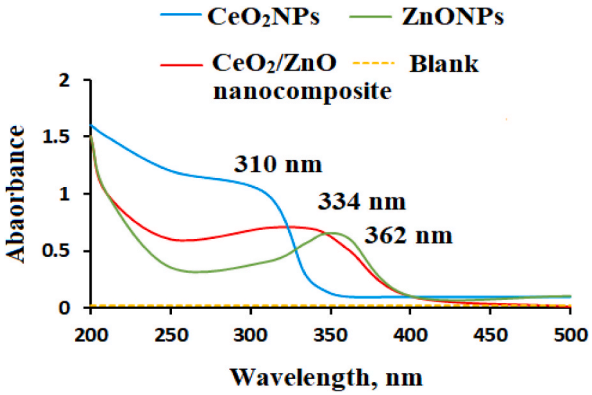

Fig. 1. UV–vis absorption spectra of green synthesized CeO_2NPs (barley husk extract), ZnONPs (rice husk extract), and CeO_2/ZnO nanocomposite, respectively measured in the range of 200–500 nm wavelength at room temperature. (For interpretation of the references to color in this figure legend, the reader is referred to the Web version of this article.)

3. Results and discussion

3.1. Characterization of the synthesized nanoparticles

Understanding the electrical structure of the optical band gap of the nanomaterials can be conducted with the aid of a spectrum analysis of UV–visible absorption. Electronic transitions inside the sample cause absorption in the near UV range. The UV–vis absorption spectra of the pre-synthesized CeO_2NPs, ZnONPs, and CeO_2/ZnO nanocomposite were measured in the wavelength range of 200–500 nm (Fig. 1). The obtained results revealed the presence of three significant bands at 310, 362, and 334 nm for the pre-synthesized nanoparticles, respectively. Accordingly, the optical band gap energy (Eg) can be calculated from absorption coefficient (A) following the Tauc equation $\alpha h\upsilon = A\,(h\upsilon\text{-}Eg)^q$ where, A, hυ, and q represent a constant that depends on the probability of transition, the transition energy of the incident photon and q the index that determines the optical absorption process. The calculated band gaps were found to be 3.97 eV, 3.16 eV, and 3.71 eV for the above-mentioned nanomaterials, respectively.

A reduction form is provided to the surface by the surface plasmon resonance (SPR), which also increases scattering likelihood and radiation penetration. These processes involve the surface-level creation of holes and the separation of electrons, which enhances the oxidation process. Additionally, it has been demonstrated that modifications to the dielectric matrix can affect the absorbance peak that appears on an SPR. The effective dielectric behavior of the matrix is known to possess a direct relationship with the refractive index.

The probable functional groups that can be found in the formed metal oxide nanomaterials were revealed by applying FTIR investigation. The FTIR spectra of CeO_2 NPs and ZnONPs displayed a series of absorption bands ranging from 400 to 4400 cm^{-1} (Fig. 2). The absorption bands at 3448 and 3450 cm^{-1} corresponded to the O–H stretching vibration of water molecules. Two absorption bands at 2370 and 2367 cm^{-1} related to C=O=C carbon dioxide of the surrounding medium. The vibration stretching bands at the ranges 615-459 cm^{-1} and 907-467 cm^{-1} expressed the presence of Ce–O and ZnO, respectively. Meanwhile, other absorption bands observed at 1622 and 1619 cm^{-1} represent the C=C stretching vibration of conjugated alkene. The recorded bands at 1044 cm^{-1} in both CeO_2NPs and ZnONPs may correspond to strong S=O stretching sulfoxide.

Different absorption bands were visible in the CeO_2/ZnO nanocomposite spectrum at wavelengths of 3450 cm^{-1} (*O*–H), 2366 cm^{-1} (O=C=O of carbon dioxide), and 1630 cm^{-1} (*O*–H vibration mode of water). The appearance of stretching vibration peaks at 574 and 466 cm^{-1} corresponds to CeO_2/ZnO nanocomposite. The inclusion of CeO_2 nanoparticles on the surface of ZnO nanoparticles is shown by the shift of the peaks in the nanocomposite spectra to 574 and 466 cm^{-1}.

X-ray diffraction detection of CeO_2NPs, ZnONPs, and their CeO_2–ZnO nanocomposite was depicted in Fig. 3a–c. Significant diffraction peaks were observed at the 2θ position of 28.16° (1 1 1), 33.35° (2 0 0), 48.38° (2 2 0),57.74° (3 1 1), 59.03° (2 2 2), 69.37° (4 0 0), 76.69° (3 3 1), and 79.09° (4 2 0) crystal planes revealed the crystalline phase of CeO_2NPs and matched the standard card no 96-900-9009 [56]. According to the XRD planes, cerium dioxide nanoparticles have a ball-like structure with a 160.54 $Å^3$ (Fig. 3a). The produced XRD pattern of ZnONPs was measured in the range of 10–100° and displayed various crystalline peaks at 31.11° (1 0 0), 34.47° (0 0 2), 36.37° (1 0 1), 47.64° (1 0 2), 55.31° (1 1 0), 63.13° (1 0 3) and 69.39° (1 1 2). When compared to the structure of zinc oxide wurtzite (JCPDS Data Card No: 36–1451), all of the observed peaks were hexagonal crystalline [57]. No additional XRD peaks except zinc oxide peaks were found, which further demonstrated that the generated ZnONPs were free of impurities (Fig. 3b). In CeO_2/ZnO nanocomposite XRD pattern the same peaks as present in Fig. 3a and b were presented revealing the loaded of CeO_2NPs on the surface of ZnONPs forming nanocomposite. The black star in Fig. 3c expressed the presence of Zn–O nanoparticles, however, the blue star expressed the existence of Ce–O nanoparticles. Debye–Scherrer formula $(D) = 0.9\lambda\ \beta \cos\theta$ [58] was followed to estimate the average crystallite size of the pre-synthesized nanoparticles, where D, β, θ, and λ were the average crystallite size, Line broadening in radians, Bragg angle, and X-Ray wavelength. The values of average crystallite size $(D) = 0.9\lambda\ \beta \cos\theta$ were found to be 17.82 ± 1.2, 17.97 ± 2.3, and 18.20 ± 1.5, for CeO_2NPs, ZnONPs, and CeO_2/ZnO nanocomposite, respectively.

SEM was used to study the morphological structure of the green synthesized nanomaterials measured at 30,000× magnification.

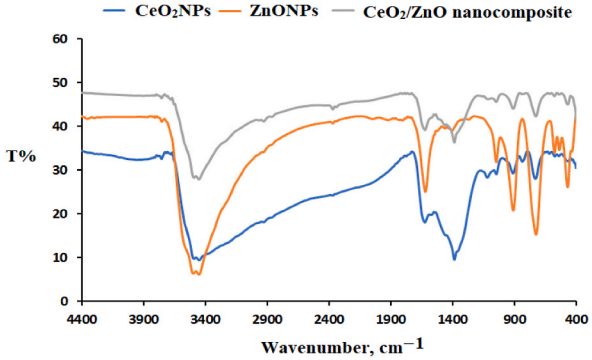

Fig. 2. FTIR spectra of UV–vis absorption spectra of green synthesized CeO_2NPs (barley husk extract), ZnONPs (rice husk extract), and CeO_2/ZnO nanocomposite, respectively measured in the range of 400–4400 cm^{-1} at room temperature. (For interpretation of the references to color in this figure legend, the reader is referred to the Web version of this article.)

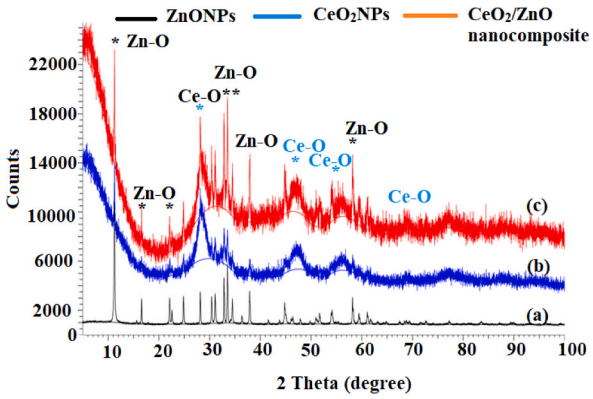

Fig. 3. XRD patterns of biogenic synthesized (a) ZnONPs (rice husk extract), (b) CeO_2NPs (barley husk extract), and (c) CeO_2/ZnO nanocomposite measured at the range 10–100°.

The obtained images confirmed the presence of CeO_2 nanoparticles in ball-like structure (Fig. 4a) and ZnO nanoparticles are in hexagonal shape (Fig. 4b).

However, CeO_2/ZnO nanocomposite exhibit hexagonal nanoparticles with spherical agglomeration revealing the appearance of CeO_2NPs on the surface of ZnONPs (Fig. 4c). The size of the formed metal oxide nanoparticles was found to be around 100 nm.

SEM coupled with an EDX spectrometer was utilized to determine the elemental content and mapping of the green synthesized CeO_2NPs (barley husk extract), ZnONPs (rice husk extract), and their CeO_2/ZnO nanocomposite. With respect to the findings in the EDX spectrum of CeO_2NPs, the weight % of the elemental content of Ce, Zn, and O was recorded as 35.9% and 64.1% for Ce and O, respectively. The atomic % was found to be 16.9% and 83.1% for the same element, respectively (Fig. 5a). The recorded data revealed that for ZnONPs the weight% was recorded as 73.7% and 26.3% for Zn and O, respectively. However, the atomic% was found to be 40.7% and 59.3% for the same elements, respectively (Fig. 5b). Moreover, The EDX spectrum of CeO_2/ZnO nanocomposite showed the presence of Ce, Zn, and O with a weight% of 10.5%, 67.2%, and 22.3% and atomic % of 2.3%, 34.6%, and 63.1% for the three elements, respectively (Fig. 5c).

3.2. *The response characteristics of the created sensors*

The critical performance and the general properties of the sensor are specified by figuring out the sensitivity, detection limit, linear

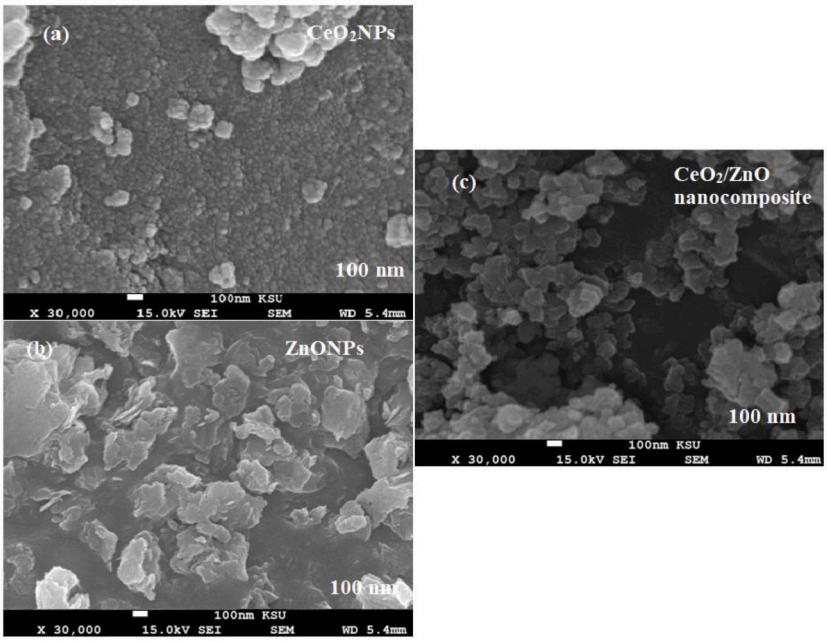

Fig. 4. SEM images of green synthesized (a) CeO_2NPs (barley husk extract), (b) ZnONPs (rice husk extract), and (c) CeO_2/ZnO nanocomposite measured at 30,000× magnification.

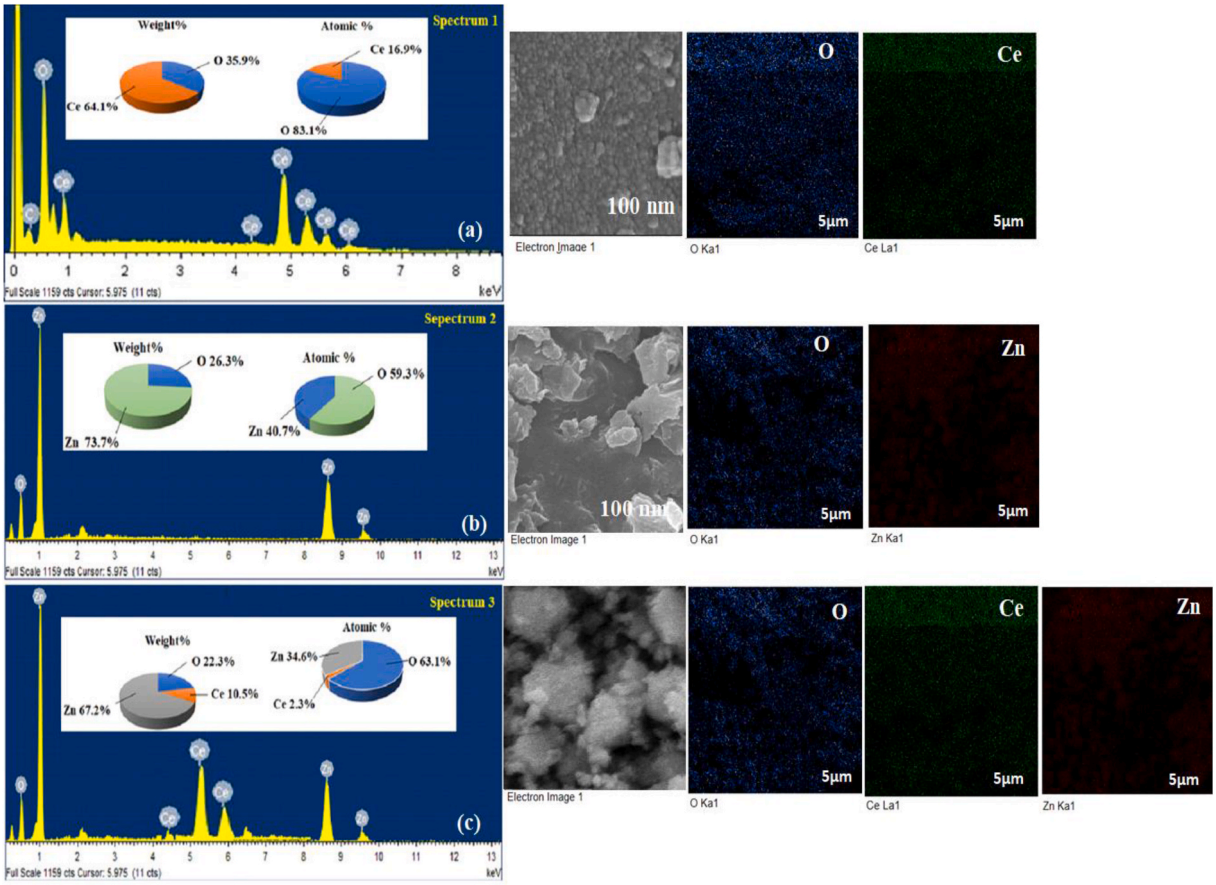

Fig. 5. EDX and mapping of green synthesized (a) CeO_2NPs (barley husk extract), (b) ZnONPs (rice husk extract), and (C) CeO_2/ZnO nanocomposite. (For interpretation of the references to color in this figure legend, the reader is referred to the Web version of this article.)

range, and selectivity coefficients of the sensor.

The potential difference between the active sites (PTD-RK or PTD-RK-CeO_2/ZnO nanocomposite) and the PTD ions in the analytical sample was used to generate the potential response of the developed sensors. The flexibility of coated membranes and their toughness is improved by adding *o*-NPOE as a plasticizer during preparation. The best response of the sensors fabricated using *o*-NPOE as a solvent mediator can be attributed to the superior dielectric properties of *o*-NPOE ($\varepsilon = 23.6$) and its capacity to extract pethidine ions from the aqueous solution. Additionally, the presence of a plasticizer can act as an ionophore due to its functional groups and donation sites, which can influence how the principal analyte ion is chelated [59].

Throughout the detection using potentiometric sensors, the response time should be considered. Thus, by immersing the sensor repeatedly in a series of solutions with a 10-fold change in concentration, the average reaction time needed for the sensor to reach a potential response within 1 mV of initial equilibrium values was determined for each sensor. The investigation of the PTD solution in the range of 1.0×10^{-9}-1.0×10^{-2} mol L^{-1} revealed that the response to reach internal equilibrium value 35, 10 s, for PTD-RK and

Table 1
The potential behavior and performance properties of PTD-RK and PTD-RK-CeO_2/ZnO nanocomposite sensors.

Parameters	Normal PTD-RK sensor	PTD-RK-CeO_2/ZnO nanocomposite sensor
Slope (mV. Decade $^{-1}$)	55.685 ± 0.1	59.107 ± 0.04
Intercept	378.27	678.96
Regression	E_{mV}=(55.685 ± 0.1)log [PTD]+378.27	E_{mV}=(59.107 ± 0.04)log [PTD]+678.96
Correlation coefficient, r	0.9995	0.9999
Linear range (mol L^{-1})	1.0×10^{-5}-1.0×10^{-2}	1.0×10^{-9}-1.0×10^{-2}
LOD	5.0×10^{-6}	4.8×10^{-10}
Response time/s	35	10
Working pH range	2–7	2–7
Lifetime/day	30	65
Temperature (°C)	25	25
Accuracy	98.83 ± 0.8	99.67 ± 0.6

PTD-RK-CeO_2/ZnO nanocomposite, respectively (Table 1).

The measurements recorded to determine the distinctive behavior of the newly developed PTD-RK or PTD-RK-CeO_2/ZnO nanocomposite sensors were summarized in Table 1. According to the collected data, the constructed sensors displayed Nernstian slopes of 55.685 ± 0.1 and 59.107 ± 0.04 mV decade^{-1}, covering 1.0 × 10^{-5}-1.0 × 10^{-2} and 1.0 × 10^{-9}-1.0 × 10^{-2} mol L^{-1}, respectively (Fig. 6a–b).

The potentials of the designed PTD-RK and PTD-RK-CeO_2/ZnO sensors were tested for their pH dependence in solutions containing 1.0 × 10^{-5} mol L^{-1} PTD spanning the pH range of 2–10. Small amounts of (1.0 mol L^{-1} HCl or NaOH) were added in small quantities to the test solutions to change the acidity, and the fluctuation in potential was monitored. The potential response is nearly consistent over the pH range of 2–7, which is considered to be the operating pH range of the suggested sensors (Fig. 7).

At pH levels lower than 1–10, there is a minor divergence, which may be caused by H^+ interference. On the other hand, at pH levels greater than 7, the potential gradually declines. This decline could be explained by the development of free PTD base and the increase of OH^- ions in the test solution [60].

Selectivity coefficients are frequently used to explain the impact of interfering chemicals on the response behavior of a selective membrane sensor. By using the separation solution technique and concentration of interference chemicals at 1.0 × 10^{-3} mol L^{-1} PTD, the selectivity coefficients for PTD with regard to a variety of interfering substances including, amino acids (glycine and histidine), cations (Mg^{2+}, Ca^{2+}, Ti^{4+}, Na^+, Cu^{2+}, Cr^{3+}, K^+, Al^{3+}, and Zn^{2+}), sugars (lactose and sucrose), and other narcotic medications (naltrexone hydrochloride, nalbuphine hydrochloride, and tramadol hydrochloride) were calculated and assessed. Table 2 provides an overview of the determined selectivity coefficients for PTD. It was clear from the results that the suggested sensors were quite selective with regard to a range of different chemicals. The functionalization of the membrane by adding CeO_2NPs and ZnONPs improves the selectivity of the sensor towards the tested analyte due to the minimized particle size and advanced physicochemical features of metal oxide nanostructures. The PTD $^+$ free energy transfer between the active sites in the membrane and the medium is often used to recognize the selectivity of the developed PTD-RK and PTD-RK-CeO_2/ZnO nanocomposite coated sensors. No significant interferences were observed due to the variance in the ionic size, mobility, and permeability of PTD^+ and interferent ions.

3.3. Quantification of pethidine hydrochloride

The proposed PTD-RK and PTD-RK-CeO_2/ZnO nanocomposite sensors were utilized to assay PTD in its authentic samples and the collected data were estimated as mean percentage recoveries. Table 3 summarized the results as 98.92 ± 0.6 and 99.69 ± 0.4 for the above-designed sensors, respectively. The addition of CeO_2/ZnO nanocomposite enhanced the stability of the designed sensor in contrast to their bulk counterparts, nanocomposite composed of CeO_2NPs and ZnONPs with large surface area to the volume have excellent electrochemical properties. Additionally, the ion-exchange surface area is increased and electron transfer between the inner sensor and the active membrane sites is improved due to the existence of the metal oxide nanocomposite.

3.4. Method validation

The validity and suitability of the constructed potentiometric systems were ensured by following the ICH recommended guidelines [61]. The developed sensors showed linearity covering 1.0 × 10^{-5}-1.0 × 10^{-2} and 1.0 × 10^{-9}-1.0 × 10^{-2} mol L^{-1} for PTD-RK and PTD-RK-CeO_2/ZnO nanocomposite sensors, respectively. The estimated regression equations previously reported in Table 1 confirmed the high sensitivity of the sensor decorated with metal oxide nanocomposite with a correlation coefficient (r = 0.9999) rather than the PTD-RK sensor (r = 0.9995).

The limit of detection (LOD) in this study can be detected when the potential readings of the proposed PTD-RK and PTD-RK-CeO_2/ZnO nanocomposite sensors decreased by 17.8 mV. The LOD was determined to be 5.0 × 10^{-6} and 5.0 × 10^{-10} mol L^{-1} for the two sensors, respectively.

To confirm the accuracy of the suggested technique, not less than nine authentic PTD samples were investigated using the

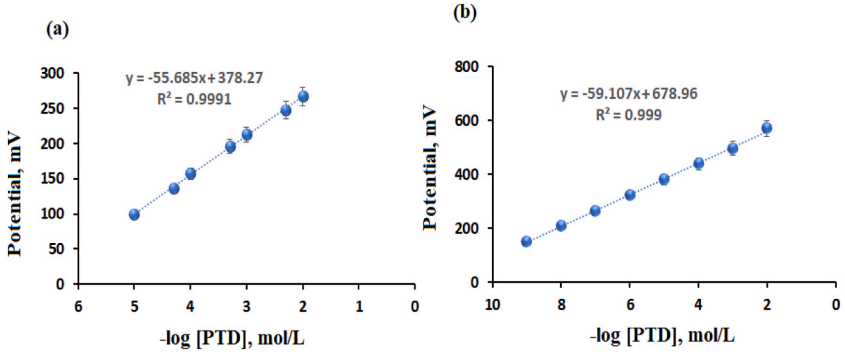

Fig. 6. Linearity graphs of (a) PTD-RK sensor using 1.0 × 10^{-5}-1.0 × 10^{-2}, (b) PTD-RK-CeO_2/ZnO nanocomposite using 1.0 × 10^{-9}-1.0 × 10^{-2} mol L^{-1} of PTD solutions.

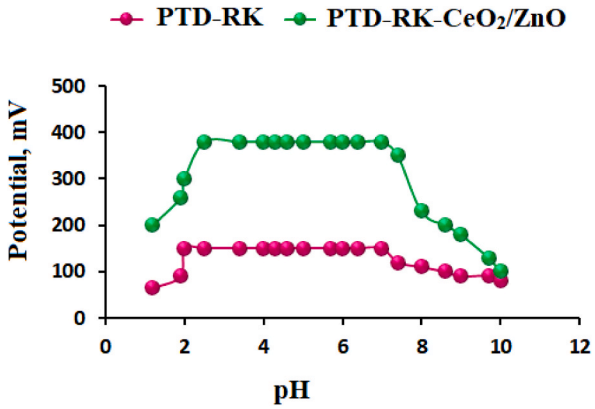

Fig. 7. The independent pH range of the suggested sensors PTD-RK and PTD-RK-CeO_2/ZnO nanocomposite using 1.0×10^{-4} mol L^{-1} PTD solution.

Table 2
Selectivity coefficient values (K^{Pot}_{PTD}) of the developed PTD-RK and PTD-RK-CeO_2/ZnO nanocomposite sensors detected by separate solution approach using 1.0×10^{-3} mol L^{-1} PTD and foreign substance solution separately.

Interferents	Conventional PTD-RK	Modified PTD-RK-CeO_2/ZnO nanocomposite sensor
Mg^{2+}	2.6×10^{-3}	3.5×10^{-4}
Ca^{2+}	4.3×10^{-3}	8.0×10^{-5}
Ti^{4+}	5.9×10^{-3}	3.2×10^{-5}
Na^{+}	3.4×10^{-3}	9.6×10^{-4}
Cu^{2+}	5.1×10^{-3}	4.3×10^{-4}
K^{+}	6.3×10^{-3}	5.2×10^{-5}
Cr^{3+}	3.9×10^{-3}	8.7×10^{-4}
Al^{3+}	2.7×10^{-3}	9.0×10^{-4}
Zn^{2+}	3.6×10^{-3}	1.6×10^{-4}
Histidine	1.4×10^{-3}	2.6×10^{-4}
Glycine	2.8×10^{-3}	3.0×10^{-5}
Sucrose	1.2×10^{-3}	4.9×10^{-5}
Lactose	5.2×10^{-3}	2.5×10^{-4}
Naltrexone hydrochloride	8.2×10^{-3}	2.6×10^{-4}
Nalbuphine hydrochloride	4.3×10^{-3}	5.8×10^{-4}
Tramadol hydrochloride	4.9×10^{-3}	1.8×10^{-4}

Table 3
The outcomes estimated from the employment of PTD-RK and PTD-RK-CeO_2/ZnO nanocomposite for the assay of PTD in its authentic samples.

Statistical analysis	PTD-RK sensor			Functionalized PTD-RK-CeO_2/ZnO nanocomposite sensor		
	Taken**	Found**	% Recovery	Taken**	Found**	% Recovery
	5	4.99	99.8	9	9.00	99.78
	4.3	4.26	99.09	8	7.97	99.87
	4	3.96	99.00	7	6.96	100.00
	3.3	3.24	98.18	6	6.00	100.00
	3	2.97	99.00	5	5.00	99.20
		1.97	98.50	4	3.98	100.00
		4.99	99.8	3	2.9	99.67
Mean ± SD n	98.92 ± 0.6			99.69 ± 0.4		
Variance	6			8		
%SE*	0.36			0.16		
%RSD	0.24			0.14		
	98.92 ± 0.6			0.40		

*SE (%Error) = SD/$\sqrt{}$ n **Taken and Found -log [PTD], mol L^{-1}.

constructed PTD-RK and PTD-RK-CeO_2/ZnO nanocomposite sensors. The accuracy was represented as mean percentage recoveries (Mean ± SD). The estimated data were 98.83 ± 0.8% and 99.67 ± 0.6% as shown in Table 4.

The precision level of the developed functionalized potentiometric was evaluated using intermediate precision (intra-day and inter-day) tests. The relative standard deviation percentage (RSD%) was used to express the estimated results. Table 5 summarized the results, which were 0.7% and 0.2% for intra- and inter-day assays, respectively, indicating excellent precision (<2%).

By utilizing phosphate to raise the pH to 7 ± 1, the resilience of the design system was assessed. The results were calculated to be

Table 4
The findings of accuracy from the determination of nine authentic samples of PTD using PTD-RK and PTD-RK-CeO_2/ZnO nanocomposite sensors.

Statistical analysis	Conventional PTD-RK sensor			Modified PTD-RK-CeO_2/ZnO nanocomposite sensor		
	Taken**	Found**	% Recovery	Taken**	Found**	% Recovery
	5	4.94	98.8	9	8.99	99.88
	4.3	4.26	99.06	8.3	8.3	100.00
	4.05	4.05	100.00	8	7.97	99.62
	4	3.96	99.00	7	7.00	100.00
	3.3	3.26	98.78	6	5.99	99.93
	3.05	3.05	100.00	5	4.98	99.60
	3	2.94	98.00	4	4.00	100.00
	2.3	2.25	97.83	3	3.00	100.00
	2	1.96	98.00	2	1.96	98.00
Mean ± SD n	98.83 ± 0.8			99.67 ± 0.6		
Variance	9			9		
%SE*	0.64			0.36		
%RSD	0.26			0.20		
	0.81			0.60		

*SE (%Error) = SD/$\sqrt{}$ n **Taken and Found -log [PTD], mol L^{-1}.

98.16 ± 0.5 and 99.76 ± 0.3% for the aforementioned two sensors, respectively. Another pH meter was used to assess the robustness of the current method (Jenway-3510). For the tested sensors, the acquired results were 98.65 ± 0.7% and 99.66 ± 0.2%. These findings showed that there was no discernible difference between the actual results and those from the analytical analyses.

3.5. Quantification of the drug in pethidine injection

PTD was determined in its commercial pharmaceutical injections. Table 6 summarized the calculated mean percentage recoveries of the analyzed samples using the functionalized PTD-RK-CeO_2/ZnO nanocomposite sensor exhibited more favorable sensitivity towards the detection of PTD analyte more than the unmodified one.

The suitable functionalization of the PTD-RK sensor with the CeO_2/ZnO nanocomposite exhibited efficient quantification of the target drug. This is owing to the advanced optical and conductive features of the green synthesized metal CeO_2NPs and ZnONPs. The large surface area and the minimized particle size, improve the interfacial connection between the target ions and the electroactive sites in the coated membrane and enhance the dynamic response, and provide excellent sensor stability [63]. The outcomes were compared with others from the previously reported sensors for the determination of PTD [19]. The results showed good agreement with no noticed significant difference.

Another comparative investigation was carried out between the functionalized PTD-RK-CeO_2/ZnO nanocomposite with previous reports according to the type of sensor, linear detection range, and lower limit of detection. The first study in Table 7 suggested the formation of a plastic membrane sensor based on phosphomolybdic acid to determine the PTD sample. The results showed that the activity of the suggested sensor covered the linear concentration range of 1.0×10^{-5}-1.0×10^{-2} mol L^{-1} with a detection limit of 5.0×10^{-6} mol L^{-1}. Whereas, the second study reported the fabrication of polymeric membrane sensor-based-silicotungstic acid with a linear concentration range of 1.0×10^{-5}-1.0×10^{-2} mol L^{-1} and LOD of 9.9×10^{-7} mol L^{-1}. Further study suggested the formation of a carbon paste electrode using phosphotungstic acid. A slight increase in the detection was observed and the measured linear concentration range was found to be 2.1×10^{-6}-1.0×10^{-2} mol L^{-1} with a detection limit of 7.3×10^{-7} mol L^{-1}. Another report showed the construction of polyvinyl chloride membrane sensor based on phosphotungstic acid to form the electroactive material. The obtained results were found to be 5.0×10^{-6}-1.0×10^{-2} mol L^{-1} and 8.2×10^{-7} mol L^{-1} for the linearity and detection limit, respectively. The present sensor in this study using functionalized PTD-RK-CeO_2/ZnO nanocomposite sensor exhibits excellent selectivity, sensitivity, and fast dynamic response due to the previously explained unique properties of the nanomaterials.

Furthermore, Hadi et al. addressed only one study on the simple biogenic synthesis of perovskite-type nanocomposite employing

Table 5
Findings of precision determined of three PTD concentrations using PTD-RK-CeO_2/ZnO nanocomposite sensor.

Statistical analysis	Functionalized PTD-RK-CeO_2/ZnO nanocomposite sensor					
	Intra-day assay			Inter-day assay		
	Taken	Found	% Recovery	Taken	Found	% Recovery
	5	4.97	99.40	9	8.99	99.88
	4	3.96	99.00	6	6.00	100.00
	2	1.96	98.00	3	2.99	99.67
Mean ± SD n	98.80 ± 0.7			99.85 ± 0.2		
Variance	3			3		
%SE	0.49			0.04		
%RSD	0.40			0.12		
	0.71			0.20		

Table 6
Detection of PTD concentrations in pethidine® (50 mg/1 mL ampoule) samples using PTD-RK and functionalized PTD-RK-CeO_2/ZnO nanocomposite sensors.

Statistical analysis	Pethidine® (50 mg/1 mL ampoule)					
	PTD-RK sensor			PTD-RK-CeO_2/ZnO nanocomposite sensor		
	Taken	Found	% Recovery	Taken	Found	% Recovery
	5	4.96	99.20	9	9.00	100.00
	4.3	4.24	98.60	8	8.00	100.00
	4	4.00	100.00	6	5.99	99.83
	3.3	3.26	98.78	4	3.97	99.25
	3	2.98	99.33	3	3.00	100.00
	2	1.96	98.00	2	1.99	99.50
Mean ± SD n	98.98 ± 0.7			99.76 ± 0.3		
Variance	6			6		
%SE	0.49			0.09		
%RSD *t*-test	0.29			0.12		
F-test	0.71			0.30		
	1.149 (2.228)*			1.458 (2.228)*		
	1.96 (5.05)*			2.78 (5.05)*		
Reported method [19]	99.42 ± 0.5					
	6					
	0.25					
	0.20					

**SE (%Error) = %RSD/$\sqrt{n}$.
***The tabulated values of ''t'' and ''F'' at confidence level $p = 0.05$ [62].

Table 7
Comparative evaluation between the findings obtained from the estimation of PTD using functionalized PTD-RK-CeO_2/ZnO nanocomposite sensor and the previously addressed potentiometric sensors.

Analytical Techniques	Reagent	Linearity	LOD	Reference
Potentiometric plastic membrane	Phosphomolybdic acid	1.0×10^{-5}-1.0×10^{-2} mol L^{-1}	5.0×10^{-6} mol L^{-1}	[16]
Potentiometric polymeric membrane	Silicotungstic acid	1.0×10^{-5}-1.0×10^{-2} mol L^{-1}	9.9×10^{-7} mol L^{-1}	[17]
Carbon paste electrode	Phosphotungstic acid	2.1×10^{-6}-1.0×10^{-2} mol L^{-1}	7.3×10^{-7} mol L^{-1}	[18]
Polyvinyl plastic membrane	Phosphotungstic acid	5.0×10^{-6}-1.0×10^{-2} mol L^{-1}	8.2×10^{-7} mol L^{-1}	[19]
Modified coated wire sensor	PTD-RK-CeO_2/ZnO nanocomposite	1.0×10^{-9}-1.0×10^{-2} mol L^{-1}	4.8×10^{-10} mol L^{-1}	Current study

Crataegus and walnut leaf extract for electrochemical assay of morphine [64]. According to this investigation, the developed system was successfully used in the detection of morphine with a limit of detection less than 1.0×10^{-8} mol L^{-1}, with percentage recovery of 96%. As previously stated, the current study using the PTD-RK-CeO2/ZnO nanocomposite demonstrated a higher sensitive detection limit of 4.8×10^{-10} mol L^{-1} with a fast dynamic response and a high percentage recovery of 99.76% for PTD determination than that reported for morphine.

4. Conclusion

The developed study described PTD-RK and PTD-RK-CeO_2/ZnO nanocomposite sensors for the determination of PTD in authentic and commercial products. The extraordinary and improved properties of the modified metal oxide CeO_2/ZnO nanocomposite coated membrane sensor exhibited excellent detection of PTD with linearity covering 1.0×10^{-9}-1.0×10^{-2} mol L^{-1} and lower limit of detections of 4.8×10^{-10} mol L^{-1} when compared with 1.0×10^{-5}-1.0×10^{-2} mol L^{-1} and lower limit of detection of 5.0×10^{-6} mol L^{-1} for the conventional PTD-RK sensor. Furthermore, developed PTD-RK and PTD-RK-CeO_2/ZnO nanocomposite sensors showed percentage recoveries of (98.92 ± 0.6 and 99.69 ± 0.4) and (98.98 ± 0.7 and 99.76 ± 0.3), respectively. In terms of selectivity, the constructed modified sensor showed better dynamic response with no significant interferences with foreign species than the existing regular sensor. The addition of metal oxide can also be used by pharmaceutical companies, and research labs to monitor PTD on a regular basis. The proposed sensor opens a promising field in the development of nanosensors that are capable of detecting the lowest concentrations of prohibited and unauthorized drugs in sports.

Author contribution statement

Suliman Y. Al Omar: Conceived and designed the experiments; Performed the experiments; Analyzed and interpreted the data; Contributed reagents, materials, analysis tools or data; Wrote the paper. Amal M. Al-Mohaimeed: Analyzed and interpreted the data; Contributed reagents, materials, analysis tools or data; Wrote the paper. Maha F. El-Tohamy: Perform the experiments; Analyzed and interpreted the data; Wrote the paper.

Data availability statement

All data of this study included within the text.

Declaration of interest's statement

The authors declare no conflict of interest.

Acknowledgment statement

The authors extend their appreciation to the Deputyship for Research & Innovation, Ministry of Education in Saudi Arabia for funding this research. (IFKSURC-1-5802).

References

[1] D. Rani, Drugs, doping and their effects on sports performance, Int. J. Economic Pers. 16 (2022) 21–31.
[2] A. Lohan, Doping and stimulants in sports: a menace and threat, Asian J. Multidimen. Res. 10 (2021) 62–69.
[3] D.B. Anderson, C.A. Shaheed, Medications for treating low back pain in adults. evidence for the use of paracetamol, opioids, nonsteroidal anti-inflammatories, muscle relaxants, antibiotics, and antidepressants: an overview for musculoskeletal clinicians, J. Orthop. Sports Phys. Ther. 52 (2022) 425–431.
[4] M.D. Bedrin, R.M. Putko, J.F. Dickens, Analgesia in athletes: a review of commonly used oral and injectable modalities, Sports Med. Arthrosc. Rev. 29 (2021) e71–e76.
[5] F. Martini, L. Fregna, M. Bosia, G. Perrozzi, R. Cavallaro, Substance-related disorders, in: Fundamentals of Psychiatry for Health Care Professionals, Springer, 2022, pp. 263–295.
[6] U. Rakip, A. Bilir, E.S. Arikan, Effect of pethidine hydrochloride on the development of neural tube: a genetic analysis study in a chick embryo model, World Neurosurg 150 (2021) e613–e620.
[7] F.R. Oguya, P.R. Kenya, F. Ongecha, P. Mureithi, Rapid situational assessment of people who inject drugs (PWID) in Nairobi and coastal regions of Kenya: a respondent driven sampling survey. http://hdl.handle.net/123456789/1793.
[8] G. Berrsche, H. Schmitt, Pain prevalences and analgesic use in junior athletes–a recent narrative review, Pain 73 (2022) 93–97.
[9] N.D. Devi, M. Putta, Y.S. Sree, P. Naveena, P. Sravani, A novel bio-analytical method for development of Pethidine in human plasma by RP-HPLC method, Pharm. Net 6 (2015) 2834–2835. http://www.pharmanest.net/.
[10] Z. Zhang, C. Zhang, X. Su, M. Ma, B. Chen, S. Yao, Carrier-mediated liquid phase microextraction coupled with high performance liquid chromatography for determination of illicit drugs in human urine, Anal. Chim. Acta 621 (2008) 185–192.
[11] Y. Huang, H. Zhang, C. Wei, G. Li, Q. Wu, J. Wang, Y. Song, Assisted sonocatalytic degradation of pethidine hydrochloride (dolantin) with some inorganic oxidants caused by CdS-coated ZrO_2 composite, Sep. Purif. Technol. 172 (2017) 202–210.
[12] A. Ishii, M. Tanaka, R. Kurihara, K. Watanabe-Suzuki, T. Kumazawa, H. Seno, O. Suzuki, Y. Katsumata, Sensitive determination of pethidine in body fluids by gas chromatography–tandem mass spectrometry, J. Chromatogr. B 792 (2003) 117–121.
[13] M.L. Zhang, X. Lin, X.R. Zhao, X.T. Lou, D.Y. Lin, Z.W. Lu, Rapid and simple detection of pethidine hydrochloride injection using surface-enhanced Raman spectroscopy based on silver aggregates, Anal. Methods 7 (2015) 8241–8247.
[14] Z. Khorablou, F. Shahdost-Fard, H. Razmi, Voltammetric determination of pethidine in biofluids at a carbon cloth electrode modified by carbon selenide nanofilm, Talanta 239 (2022), 123131.
[15] H. Shahinfard, M. Shabani-Nooshabadi, A. Reisi-Vanani, H. Ansarinejad, A novel platform based on $CoMn_2O_4$-rGO/1-ethyl-3-methylimidazolium chloride modified carbon paste electrode for voltammetric detection of pethidine in the presence morphine and olanzapine, Chemosphere 301 (2022), 134710.
[16] A. Shalaby, M. El-Tohamy, M. Elmaamly, H.Y. Aboul-Enein, Potentiometric membrane sensor for the selective determination of pethidine in pharmaceutical preparations and biological fluids, Ann. Chim. (Rome, Italy) 97 (2007) 1065–1074.
[17] Z.H. Liu, M.L. Wen, J. Xiong, A pethidine selective polymeric membrane electrode based on pethidine silicotungstate, Anal. Sci. 16 (2000) 885–887.
[18] H.M. Abu-Shawish, N. Abu Ghalwa, G.I. Khraish, J. Hammad, A new potentiometric sensor for determination of pethidine hydrochloride in ampoules and urine, Am. J. Anal. Chem. 2 (2011).
[19] Z.H. Liu, M.L. Wen, Y. Yao, J. Xiong, Plastic pethidine hydrochloride membrane sensor and its pharmaceutical applications, Sens. Actuators, B 72 (2001) 219–223.
[20] Z.H. Liu, M.L. Wen, Y. Yao, J. Xiong, A Pethidine selective polymeric membrane electrode, Boletin de la Soc. Chil. de Quim. 47 (2002) 163–168.
[21] H.M. Abu-Shawish, A.A. Dalou, N.A. Ghalwa, G.I. Khraish, J. Hammad, A.H. Basheer, Determination of pethidine hydrochloride using potentiometric coated graphite and carbon paste electrodes, Drug Test. Anal. 5 (2013) 213–221.
[22] H.M. Abu-Shawish, A New potentiometric sensor for determination of pethidine hydrochloride in ampoules and urine, Am. J. Anal. Chem. 2 (2011) 56–65.
[23] O. Ozbek, O. Isildak, I. Isildak, A potentiometric biosensor for the determination of valproic acid: human blood–based study of an anti–epileptic drug, Biochem. Eng. J. 176 (2021), 108181.
[24] S.S. Alterary, M.F. El-Tohamy, Advanced functionalized CeO_2/Al_2O_3 nanocomposite sensor for determination of opioid medication tramadol hydrochloride in pharmaceutical formulations, Nanomaterials 12 (2022) 1373.
[25] S.S. Alterary, M.F. El-Tohamy, G.A. Mostafa, H. Alrabiah, Atropine-phosphotungestate polymeric-based metal oxide nanoparticles for potentiometric detection in pharmaceutical dosage forms, Nanomaterials 12 (2022) 2313.
[26] X. Xia, S. Zhao, H. Yin, G.J. Weng, Revealing the AC electromechanically coupled effects and stable sensitivity on the dielectric loss in CNT-based nanocomposite sensors, Mater. Des. 216 (2022), 110557.
[27] M. Panda, N. Sultana, A.K. Singh, Structural and optical properties of PVDF/GO nanocomposites, Fullerenes, Nanotub. Carbon Nanostruct. 30 (2022) 559–570.
[28] H. Wang, J. Xiang, X. Wen, X. Du, Y. Wang, Z. Du, X. Cheng, S. Wang, Multifunctional skin-inspired resilient MXene-embedded nanocomposite hydrogels for wireless wearable electronics, Compos. Appl. Sci. Manuf. 155 (2022), 106835.
[29] T. Khani, Z. Alamzadeh, A. Sarikhani, M. Mousavi, M. Mirrahimi, M. Tabei, R. Irajirad, Z. Abed, J. Beik, Fe_3O_4@ Au core–shell hybrid nanocomposite for MRI-guided magnetic targeted photo-chemotherapy, Laser Med. Sci. (2022) 1–9.
[30] M. Amina, N.M. Al Musayeib, N.A. Alarfaj, M.F. El-Tohamy, G.A. Al-Hamoud, Antibacterial and anticancer potentials of pre-synthesized photosensitive *Plectranthus cylindraceus* Oil/TiO_2/polyethylene glycol polymeric bionanocomposite, Bioinorgan. Chem. Appl. 2021 (2021), 5562206.
[31] M.K. Valsakumari, N.K. Anushkannan, M. Anusuya, S.K. Chinnaiyan, B. Haldar, M. Jayapriya, K. Ramachandran, Biomolecules and microwaves directed fabrication of Ag/CeO_2 nanocomposite: a versatile candidate for the degradation of textile dye mixtures and antibacterial studies, Res. Chem. Intermed. (2022) 1–8.
[32] S. Li, Z. Zheng, Z. Zhao, Y. Wang, Y. Yao, Y. Liu, J. Zhang, Z. Zhang, CeO_2 nanoparticle-loaded MnO_2 nanoflowers for selective catalytic reduction of NOx with NH_3 at low temperatures, Molecules 27 (2022) 4863.
[33] I.K. Sani, M. Alizadeh, Isolated mung bean protein-pectin nanocomposite film containing true cardamom extract microencapsulation/CeO_2 nanoparticles/graphite carbon quantum dots: investigating fluorescence, photocatalytic and antimicrobial properties, Food Packag. Shelf Life 33 (2022), 100912.

[34] S. Sekar, C. Bathula, I. Rabani, J.W. Lee, S.H. Lee, Y.S. Seo, S. Lee, Enhanced photocatalytic crystal-violet degradation performances of sonochemically-synthesized AC-CeO_2 nanocomposites, Ultrason. Sonochem. 90 (2022), 106177.
[35] A.R. Prasad, L. Williams, J. Garvasis, K.O. Shamsheera, S.M. Basheer, M. Kuruvilla, A. Joseph, Applications of phytogenic ZnO nanoparticles: a review on recent advancements, J. Mol. Liq. 331 (2021), 115805.
[36] G.X. Wan, Y. Feng, F.F. Zhang, X.W. Sun, Y.X. Li, R.J. Xue, Hydrothermal synthesis of Ag doped ZnO/CeO_2 nanocomposites and its application in ethanol sensing, Mater. Lett. 318 (2022), 132191.
[37] K. Jan, C.S. Riar, D.C. Saxena, Characterization of agro-industrial byproducts and wastes for sustainable industrial application, Food Meas 11 (2017) 1254–1265.
[38] K. Jan, C.S. Riar, D.C. Saxena, Engineering and functional properties of biodegradable pellets developed from various agro-industrial wastes using extrusion technology, J. Food Sci. Technol. 52 (2015) 7625–7639.
[39] A. Zamani, A.P. Marjani, Z. Mousavi, Agricultural waste biomass-assisted nanostructures: synthesis and application, Green Process. Synth. 8 (2019) 421–429.
[40] E. Akhayere, A. Vaseashta D. Kavaz, Novel magnetic nano silica synthesis using barley husk waste for removing petroleum from polluted water for environmental sustainability, Sustainability 12 (2020), 10646.
[41] F. Gheitasi, S. Ghammamy, M. Zendehdel, F.B. Semiromi, Removal of mercury (II) from aqueous solution by powdered activated carbon nanoparticles prepared from beer barley husk modified with Thiol/Fe_3O_4, J. Mol. Struct. 1267 (2022), 133555.
[42] H. Gomaa, M.A. Hussein, M.M. Motawea, A.M. Aboraia, M.F. Cheira, M.T. Alotaibi, S.M. El-Bahy, H.A. Ali, A hybrid mesoporous CuO@ barley straw-derived SiO_2 nanocomposite for adsorption and photocatalytic degradation of methylene blue from real wastewater, Colloids Surf., A 644 (2022), 128811.
[43] E.C. Okonkwo, E.A. Essien, M. Abid, D. Kavaz, T.A. Ratlamwala, Thermal performance analysis of a parabolic trough collector using water-based green-synthesized nanofluids, Sol. Energy 170 (2018) 658–670.
[44] J. Athinarayanan, V.S. Periasamy, M. Alhazmi, K.A. Alatiah, A.A. Alshatwi, Synthesis of biogenic silica nanoparticles from rice husks for biomedical applications, Ceram. Int. 41 (2015) 275–281.
[45] A. Agi, R. Junin, M.Z. Jaafar, R. Mohsin, A. Arsad, A. Gbadamosi, F.C. Fung, J. Gbonhinbor, Synthesis and application of rice husk silica nanoparticles for chemical enhanced oil recovery, J. Mater. Res. Technol. 9 (2020) 13054–13066.
[46] E. Idehen, Y. Tang, S. Sang, Bioactive phytochemicals in barley, J. Food Drug Anal. 25 (2017) 148–161.
[47] Y. Gao, X. Guo, Y. Liu, Z. Fang, M. Zhang, R. Zhang, L. You, T. Li, R.H. Liu, A full utilization of rice husk to evaluate phytochemical bioactivities and prepare cellulose nanocrystals, Sci. Rep. 8 (2018), 10482.
[48] M. Yadav, V. Dwibedi, S. Sharma, N. George, Biogenic silica nanoparticles from agro-waste: properties, mechanism of extraction and applications in environmental sustainability, J. Environ. Chem. Eng. 7 (2022), 108550.
[49] N. Shahi, E. Lee, B. Min, D.J. Kim, Rice husk-derived cellulose nanofibers: a potential sensor for water-soluble gases, Sensors 21 (2021) 4415.
[50] Z. Izadiyan, K. Shameli, M. Miyake, H. Hara, S.E. Mohamad, K. Kalantari, S.H. Taib, E. Rasouli, Cytotoxicity assay of plant-mediated synthesized iron oxide nanoparticles using Juglans regia green husk extract, Arab. J. Chem. 13 (2020) 2011–2023.
[51] N.M. Ishak, S.K. Kamarudin, S.N. Timmiati, Green synthesis of metal and metal oxide nanoparticles via plant extracts: an overview, Mater. Res. Express 6 (2019), 112004.
[52] M.A. Hussein, A. Khan, K.A. Alamry, A highly efficient electrochemical sensor containing polyaniline/cerium oxide nanocomposites for hydrogen peroxide detection, RSC Adv. 12 (2022) 31506–31517.
[53] R. Shanthi, M.C. Devi, M. Abukhaled, M.F. Lyons, L. Rajendran, Mathematical modeling of pH-based potentiometric biosensor using Akbari-Ganji method, Int. J. Electrochem. Sci. 17 (2022), 2203492.
[54] H.M. Shawish, S.M. Saadeh, S.T. Al-kahlout, PVC membrane, coated-wire, and carbon-paste electrodes for potentiometric determination of vardenafil hydrochloride in tablet formulations and urine samples, Sensors Int 3 (2022), 100175.
[55] H.S. Abd-Rabboh, A.E. Amr, A.A. Almehizia, A.H. Kamel, Based potentiometric device for rapid and selective determination of salicylhydroxamate as a urinary struvite stone inhibitor, ACS Omega 6 (2021) 27755–27762.
[56] L. Baca, H. Steiner, N. Stelzer, Upconversion luminescence and optical thermometry in Er3+/Yb3+ co-doped CeO_2 for space application, J. Alloys Compd. 774 (2019) 418–424.
[57] T.M. Elmorsi, M.H. Elsayed, M.F. Bakr, Enhancing the removal of methylene blue by modified ZnO nanoparticles: kinetics and equilibrium studies, Can. J. Chem. 95 (2017) 590–600.
[58] U. Holzwarth, N. Gibson, The Scherrer equation versus the' Debye-Scherrer equation, Nat. Nanotechnol. 6 (2011) 534.
[59] A.M. Silva, M.F. Pimentel, I.M. Raimundo Jr., Y.M. Almeida, Effect of plasticizers on a PVC sensing phase for evaluation of water contamination by aromatic hydrocarbons and fuels using infrared spectroscopy, Sens. Actuators, B 139 (2009) 222–230.
[60] M. Liu, M. Jia, E. Yifeng, D. Li, A novel ion selective electrode based on reduced graphene oxide for potentiometric determination of sarafloxacin hydrochloride, Microchem. J. 170 (2021), 106678.
[61] ICH-Q2 (R1) Validation and Analytical Procedures: Text and Methodology. International Conference on Harmonization Guidelines, Geneva, November, (2005).
[62] J.C. Miller, J.N. Miller, Statistics for Analytical Chemistry, third ed., Ellis Horwood PTR Prentice Hall, New York, NY, USA, 1993.
[63] I.M. Isa, N.M. Sohaimi, N. Hashim, A. Kamari, A. Mohamed, M. Ahmad, S.A. Ghani, Determination of salicylate ion by potentiometric membrane electrode based on zinc aluminium layered double hydroxides-4(2,4-dichlorophenoxy) butyrate nanocomposites, Int. J. Electrochem. Sci. 8 (2013) 2112–2121.
[64] H. Mahmoudi-Moghaddam, M. Amiri, H.A. Javar, Q.A. Yousif, M. Salavati-Niasari, A facile green synthesis of a perovskite-type nanocomposite using Crataegus and walnut leaf for electrochemical determination of morphine, Anal. Chim. Acta 1203 (2022), 339691.